Optics Communications 294 (2013) 368–371

Contents lists available at SciVerse ScienceDirect

Optics Communications

journal homepage: www.elsevier.com/locate/optcom

Research on transmission characteristics of aperture-coupled square-ring resonator based filter

Xiao Peng [a], Hongjian Li [a,b,*], Caini Wu [a], Guangtao Cao [b], Zhimin Liu [a]

[a] College of Physics and Electronics, Central South University, Changsha 410083, China
[b] College of Materials Science and Engineering, Central South University, Changsha 410083, China

ARTICLE INFO

Article history:
Received 26 July 2012
Received in revised form
23 November 2012
Accepted 8 December 2012
Available online 8 January 2013

Keywords:
Aperture-coupled square-ring resonator
Transmission resonance
Semi-integer resonance modes

ABSTRACT

In this study, a nanometric surface plasmon polariton (SPP) filter based on an aperture-coupled square-ring resonator is presented and the transmission characteristics of the SPP filter are analyzed in detail by using the finite difference time domain (FDTD) method. Results show that lifting of degeneracy exists in both even-modes and odd-modes for the regular side-coupled square-ring resonator. By introducing the aperture between the ring and bus waveguide, semi-integer resonance modes with high drop efficiency emerge in the optical transmission spectrum. Further simulation results show that semi-integer modes can be efficiently modified and linearly tuned by adjusting the parameters of the resonators such as side length of the ring, the width of the aperture and the medium inside the aperture. The simple band-stop SPP filter is very promising for high-density SPP waveguide integrations.

1. Introduction

Surface Plasmon Polaritons (SPPs), which are electromagnetic waves propagating along the metal–dielectric interface with an exponentially decaying field in both sides, have been considered as energy and information carriers to overcome the diffraction limit of light in conventional optics, making these structures a prime candidate for miniaturized photonic integrated circuits [1–3]. In recent years, various SPPs based devices have been numerically investigated or experimentally demonstrated, such as bends [4], splitters [5], Mach–Zehnder interferometers [6], Y-shaped combiners [7], Bragg grating [8,9], side coupled Fabry–Perot cavity [10,11], tooth-shaped waveguide filters [12,13].

Recently, Hosseini and Massoud [14] proposed a side-coupled rectangular ring resonator based filter and an aperture-coupled rectangular ring resonator based filter, but the latter one is not analyzed and elucidated in detail. After that, various ring resonators based filter are proposed and numerically investigated [15,16]. Such as side-coupled and end-coupled circular ring resonator [15,16], end-coupled rectangular ring resonator [17]. Also, side-coupled and end-coupled disk resonators [18,19] were proposed and investigated. These resonators are mainly integer modes resonators with either band-stop or band-pass characteristics. More recently, Iman [20] proposed a new complementary split-ring resonator which has non-integer modes.

In this paper, we will focus on the resonance modes of the regular side-coupled square-ring resonator (RSSR) based filter and aperture-coupled square-ring resonator (ASR) based filter, which are presented and analyzed in detail by the finite difference time domain (FDTD) method. First, the transmission spectrum of the regular side-coupled square-ring resonator (RSSR) based filter is investigated. And lifting of degeneracy in both even-modes and odd-modes is observed, However, in [20], only even-modes witness lifting of degeneracy. Second, semi-integer resonance modes are observed and verified for the aperture-coupled square-ring resonator (ASR) based filter in our simulation, which has not been declared in Ref. [14], and these semi-integer modes are different from the ones in Ref. [20]. Additionally, in previous works, by varying the outer dimensions of the structure, i.e. side length of the ring, tunable filters were achieved. Here, we also modify the spectrum by changing the width of the aperture and the medium inside it without enlarging or minimize the outer parameter of the resonator. This new characteristic is beneficial in the case of integrated circuits.

2. Model and method

The finite difference time-domain (FDTD) method with the perfectly matched layer (PML) boundary conditions is used to numerically explore characteristics of the RSSR and ASR filter. In the simulations, the structure in the z direction is considered to be infinite (2D). The green and white areas are silver and air, respectively. The pink areas can be air or other dielectric medium.

* Corresponding author at: Central South University, College of Physics and Electronics, Lusan Lu 8#, Changsha, Hunan 410083, China.
E-mail address: lihj398@yahoo.com.cn (H. Li).

0030-4018/$ - see front matter © 2012 Elsevier B.V. All rights reserved.
http://dx.doi.org/10.1016/j.optcom.2012.12.026

The propagation constant β in the waveguide is determined by the dispersion relation. The dispersion relation of the fundamental TM mode in a MIM waveguide is given by [12]

$$\varepsilon_d k_{z2} + \varepsilon_m k_{z1} \coth\left(-\frac{ik_{z1}}{2}w\right) = 0 \quad (1)$$

and k_{z1} and k_{z2} are

$$k_{z1}^2 = \varepsilon_d k_0^2 - \beta^2, k_{z2}^2 = \varepsilon_m k_0^2 - \beta^2 \quad (2)$$

where ε_d, ε_m and $k_0 = 2\pi/\lambda$ are the dielectric constants of the insulator (air) and the metal (silver), and the free-space wave vector, respectively. The frequency-dependent complex relative permittivity of silver is characterized by the Drude model:

$$\varepsilon_m(\omega) = \varepsilon_\infty - \omega_p^2/(\omega^2 + i\omega\gamma) \quad (3)$$

where $\omega_p = 1.38 \times 1016$ Hz is the bulk plasma frequency which represents the natural frequency of the oscillations of free conduction electrons, $\gamma = 2.73 \times 1013$ Hz is the damping frequency of the oscillations, ω is the angular frequency of the incident electromagnetic radiation and ε_∞ stands for the dielectric constant at infinite angular frequency with a value of 3.7.

The main structural parameters of the optical filter are the side length of the rectangular MIM ring resonator in the x direction (Lx) and y direction (Ly), the width of the MIM bus waveguide ($W1$), the width of the square MIM ring resonator ($W2$), the width of the aperture ($W3$) and the barrier thickness of the coupling region between the MIM bus waveguide and the square MIM ring resonator (g). Two power monitors Pin and Pout are set to calculate the incident power of the transmitted power, and transmittance of the filter is defined as $T = P_{out}/P_{in}$. It is important to point out that, in all cases for the whole paper, the width of the waveguides $W1$ and $W2$ is set to be 50 nm to ensure that only the fundamental TM mode is supported. Coupling thickness $g = 25$ nm also keeps invariant in the whole paper.

3. Simulation results and discussion

3.1. RSSR filter

The simulated transmission spectrum of the regular side-coupled square-ring resonator (RSSR) based filter ($Lx = Ly = 225$ nm) is shown in Fig. 2 and the magnetic-field distributions at the resonance wavelengths are shown as insets in Fig. 2. Here we have studied different values for $Lx = Ly$. For others values, the splits may occur either at the even-modes or the odd-modes. But

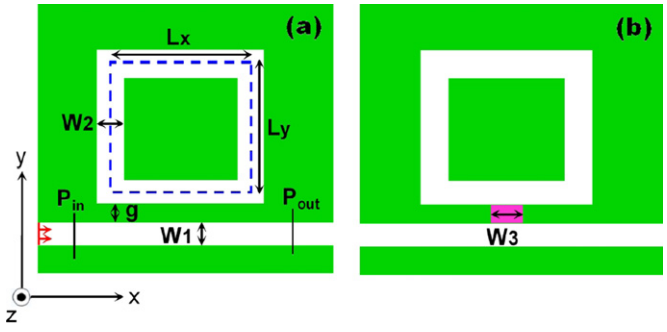

Fig. 1. (a) The structure of the regular side-coupled square-ring resonator (RSSR) based filter which is composed of an MIM bus waveguide and a MIM square-ring resonator. (b) The schematic of the aperture-coupled square-ring resonator (ASR) based filter, where a aperture is placed between the ring and the bus waveguide. (For interpretation of the references to color in this figure caption, the reader is referred to the web version of this article.)

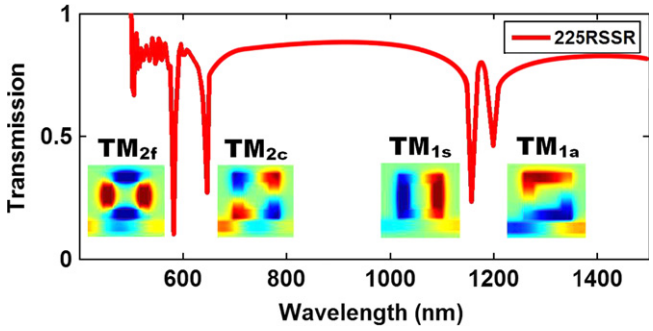

Fig. 2. The transmission spectrum of the regular side-coupled square-ring resonator (RSSR) based filter ($Lx = Ly = 225$ nm). The magnetic distributions are shown as insets.

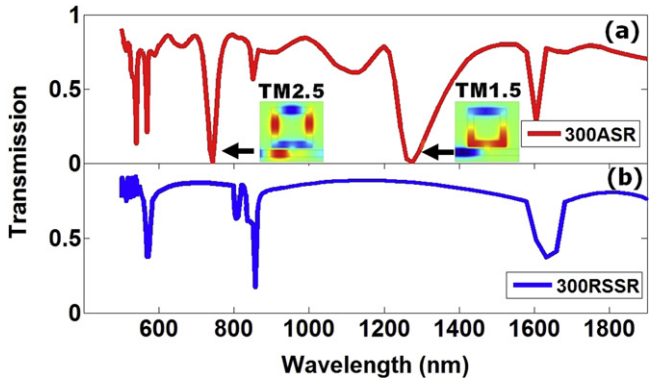

Fig. 3. The transmission spectra of ASR based filter and RSSR based filter with $Lx = 300$ nm.

it is observed that when $Lx = Ly = 225$ nm, both odd-modes and even-modes exhibit split. The total MIM waveguide length in the square-ring cavity (cavity length) in this case can be calculated by $L = 2(Lx + Ly) = 900$ nm. The resonance condition for the rectangular ring cavity is [14]

$$L = N\lambda_{spp} = N(\lambda_r/\mathrm{Re}(n_{eff})), \ (N = 1,2,3,\ldots) \quad (4)$$

where N, an integer, is the mode number. And it can be seen from Fig. 2, the wavelength of simulation results is consistent with the resonance condition on the whole, although the effective refractive index n_{eff} as a function of wavelength should be considered according to the dispersion relation [12]. For $\lambda_r = 581$ nm and $\lambda_r = 646$ nm, which poses four magnetic antinodes at the faces and corners, are denoted by TM_{2f} and TM_{2c}, respectively. For $\lambda_r = 1157$ nm and $\lambda_r = 1199$ nm, which poses two magnetic antinodes, are denoted by TM_{1s} (symmetric) and TM_{1a} (asymmetric) [20].

The possible differences in the transmission spectra between the circular ring and rectangular ring are mainly attributed to the role of the corners of a rectangular ring structure [14,21]. The corners of the square-ring can be treated as outward perturbations of the circular structure. The outward perturbation will decrease (increase) the resonance frequency if it is created at the position of a large magnetic (electric) field [20]. The corner-modes TM_{2c} (at $\lambda_r = 646$ nm) and TM_{1a} (at $\lambda_r = 1199$ nm) which have longer wavelength than that of TM_{2f} and TM_{1s} can be easily explained. It should be emphasized that, in Fig. 2, the odd-modes TM_1 split into TM_{1s} (at $\lambda_r = 1157$ nm) and TM_{1a} ($\lambda_r = 1199$ nm), which is mentioned but not observed in Ref. [20]. In this study, lifting of the degeneracy in both even-modes and odd-modes is verified.

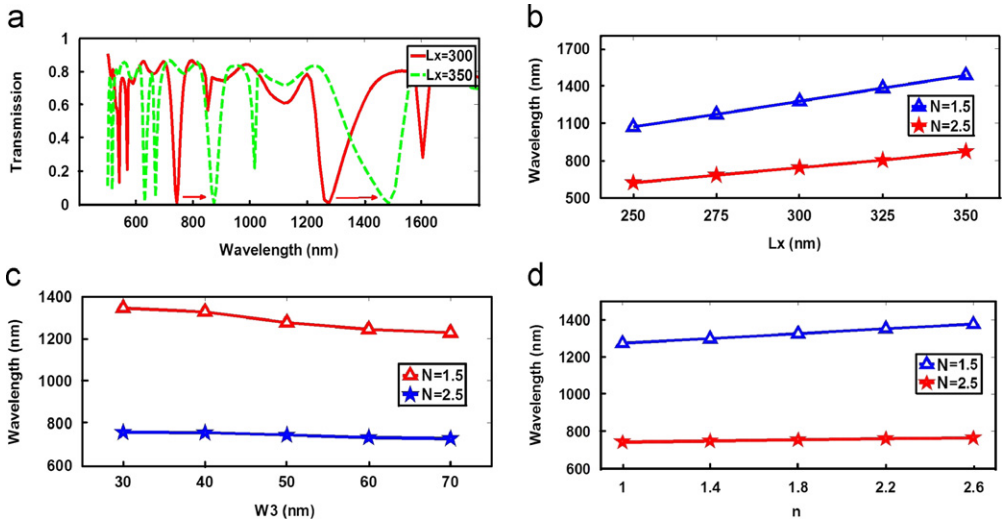

Fig. 4. (a) The transmission spectra of ASR filter with $Lx=300$ nm and $Lx=350$ nm. (b) Semi-integer mode resonance wavelength as a function of Lx. (c) Semi-integer mode resonance wavelength vs. the width of the aperture $W3$. (d) Semi-integer mode resonance wavelength vs. the dielectric constant n of the medium in the aperture.

3.2. ASR filter

In this section, the aperture-coupled square-ring resonator (ASR) based filter is studied in detail. Fig. 1(b) shows the schematic of the ASR filter. In contrast to the RSSR filter, one narrow aperture (bridge) exists between the bus waveguide and the square-ring.

Fig. 3(a) shows the transmission spectrum of the ASR filter. In Fig. 3(a) the structural parameters of the ASR filter are set to be $Lx=Ly=300$ nm, $W1=W2=50$ nm, $g=25$ nm, $W3=50$ nm. The transmission of RSSR filter with the same parameter is also plotted in Fig. 3(b). By comparing the two spectra, for ASR filter, two new resonance modes appear, while the regular integer-modes wavelengths almost stay at the same position. The magnetic-field distributions of the new drops show these modes are semi-integer modes. The resonance wavelength at 742 nm which is denoted by $TM_{2.5}$ has five magnetic antinodes. The resonance wavelength at 1276 nm, which is denoted by $TM_{1.5}$, has three magnetic antinodes. The resonance wavelengths accord with the resonance condition equation (4) in general. For $\lambda_r=742$ nm, $N=2.5$. For $\lambda_r=1276$ nm, $N=1.5$. $N=0.5$ at longer wavelength is not discussed in this paper. These semi-modes are not declared in Ref. [14]. It should be noticed that these semi-integer modes are different from the semi-interger modes in Ref. [20]. As can be seen from Fig. 3(a), magnetic field near the aperture is same-phase, however, in Ref. [20], it is anti-phase. According to the above phenomenon, by placing one aperture between the ring and the bus waveguide, new semi-integer modes can be excited. It is also worthy to notice that these semi-integer modes have higher a drop efficiency compared to the regular integer modes.

Characteristics of these semi-integer modes are investigated. One of the ways to manipulate the transmission spectra of ASR filter is by changing the side length Lx. Fig. 4(a) shows the transmission spectra of ASR filter with different Lx values of 300 nm and 350 nm. By increasing the side length Lx, the resonance exhibits a red shift for both integer and semi-integer modes. This can be explained by Eq. (4), as Lx increases, L increases, so the resonance wavelength increases. For clarity, the wavelength of the $TM_{1.5}$ and $TM_{2.5}$ as a function of side length Lx is plotted in Fig. 4(b). As Lx varies from 250 nm to 350 nm, $TM_{2.5}$ changes from 621 nm to 873 nm, while for $TM_{1.5}$ the wavelength changes from 1070 nm to 1485 nm.

Fig. 4(c) shows that by varying the width of $W3$, the resonance wavelength also can be manipulated. When increasing $W3$ from 30 nm to 70 nm, the $TM_{2.5}$ mode wavelength drops from 756 nm to 726 nm and $TM_{1.5}$ mode wavelength drops from 1345 nm to 1288 nm. This can be explained as follows: increasing the width of $W3$ equals increasing the width of part of $W2$, which means a decrease on n_{eff}. Thus, according to the resonance condition (4), the wavelength decreases. Fig. 4(d) plots the variation of semi-integer modes wavelength as a function of refractive index of the medium in the aperture. From Fig. 4(d), the transmission shift to longer wavelength as n increases. It is also easy to find, from Fig. 4(b)–(d), $TM_{1.5}$ varies more drastically than $TM_{2.5}$. This can be interpreted by the following equations derived from resonance conditions (4). $\lambda=Ln_{eff}/N$, $d\lambda_{N=1.5}/d\lambda_{N=2.5}=n_{eff1.5}/n_{eff2.5}\times 2>1$. From the above expression, we explain why in Fig. 4(b)–(d), $TM_{1.5}$ has a larger inclination value than $TM_{2.5}$.

4. Conclusion

In summary, a regular side-coupled square-ring resonator (RSSR) based filter and an aperture-coupled square-ring resonator (ASR) based filter are presented. The characteristics of the RSSR filter and ASR filter are analyzed in detail by using FDTD method. Lifting of degeneracy for both odd-mode and even-mode in the RSSR filter is observed at the first time. Semi-integer resonance modes emerge in the optical transmission spectrum for ASR filter. The effects of parameters of the resonators such as side length of the ring, the width of the aperture and the medium inside the aperture on the wavelength of semi-integer modes are discussed. Numerical calculations are consistent with theoretical analysis in general. The simple band-stop SPP filter is very promising for high-density SPP waveguide integrations.

Acknowledgments

This work was funded by the Research Fund for the Doctoral Program of Higher Education of China under Grant No. 20100162110068 and the National Natural Science Foundation of China under Grant Nos. 61275174 and 11164007.

References

[1] W.L. Barnes, A. Dereux, T.W. Ebbesen, Nature 424 (2003) 824.
[2] R. Zia, J.A. Schuller, A. Chandran, M.L. Brongersma, Materials Today 9 (2006) 20.
[3] E. Ozbay, Science 311 (2006) 189.
[4] T.W. Lee, S. Gray, Optics Express 13 (2005) 9652.
[5] G. Veronis, S. Fan, Applied Physics Letters 87 (2005) 131102.
[6] B. Wang, G.P. Wang, Optics Letters 29 (2004) 1992.
[7] H. Gao, H. Shi, C. Wang, C. Du, X. Luo, Q. Deng, Y. Lv, X. Lin, H. Yao, Optics Express 13 (2005) 10795.
[8] B. Wang, G. Wang, Applied Physics Letters 87 (2005) 013107.
[9] Z. Han, E. Forsberg, S. He, IEEE Photonics Technology Letters 19 (2007) 91.
[10] Q. Zhang, X.G. Huang, X.S. Lin, J. Tao, X.P. Jin, Optics Express 17 (2009) 7549.
[11] L. Liu, X. Hao, Optics Communications 285 (2012) 2558.
[12] X.S. Lin, X.G. Huang, Optics Letters 33 (2008) 2874.
[13] J. Tao, X.G. Huang, X.S. Lin, Q. Zhang, X.P. Jin, Optics Express 17 (2009) 13989.
[14] A. Hosseini, Y. Massoud, Applied Physics Letters 90 (2007) 181102.
[15] Z. Han, V. Van, W.N. Herman, P.T. Ho, Optics Express 17 (2009) 12678.
[16] T.B. Wang, X.W. Wen, C.P. Yin, H.Z. Wang, Optics Express 17 (2009) 24096.
[17] B. Yun, G. Hu, Y. Cui, Journal of Physics D Applied Physics 43 (2010) 385102.
[18] H. Lu, X. Liu, D. Mao, L. Wang, Y. Gong, Optics Express 18 (2010) 17922.
[19] H. Lu, X.M. Liu, Y.K. Gong, L. Wang, D. Mao, Optics Communications 284 (2011) 2613.
[20] Amirreza Iman Zand, Tavakol Mahigir, Pakizeh, S. Abrishamian, Optics Express 20 (2012) 7516.
[21] J. Liu, G. Fang, H. Zhao, Y. Zhang, S. Liu, Journal of Physics D Applied Physics 43 (2010) 055103.